ACS APPLIED MATERIALS & INTERFACES

Research Article

Cite This: ACS Appl. Mater. Interfaces 2018, 10, 15855−15863

www.acsami.org

Piezoelectric Polyacrylonitrile Nanofiber Film-Based Dual-Function Self-Powered Flexible Sensor

Gengrui Zhao,[†,‡] Xiaodi Zhang,[†,‡] Xin Cui,[§] Shu Wang,[†,‡] Zhirong Liu,[†,‡] Lin Deng,[†,‡] Anhui Qi,[†] Xiran Qiao,[†] Lijie Li,[∥] Caofeng Pan,[†,‡,§] Yan Zhang,*[,⊥,†,§] and Linlin Li*[,†,‡,§]

[†]Beijing Institute of Nanoenergy and Nanosystems, Chinese Academy of Sciences, Beijing 100083, P. R. China

[‡]School of Nanoscience and Technology, University of Chinese Academy of Sciences, Beijing 100049, P. R. China

[§]Center on Nanoenergy Research, School of Physical Science and Technology, Guangxi University, Nanning 530004, P. R. China

[∥]Multidisciplinary Nanotechnology Center, College of Engineering, Swansea University, Bay Campus, Swansea SA1 8EN, U.K.

[⊥]School of Physics, University of Electronic Science and Technology of China, Chengdu 610054, P. R. China

Supporting Information

ABSTRACT: To meet the growing demands in flexible and wearable electronics, various sensors have been designed for detecting and monitoring the physical quantity changes. However, most of these sensors can only detect one certain kind of physical quantity based on a single mechanism. In this paper, we have fabricated a multifunctional sensor made from carbonized electrospun polyacrylonitrile/barium titanate (PAN-C/BTO) nanofiber film. It can detect two physical quantities (pressure and curvature), independently and simultaneously, by integrating piezoresistive, piezoelectric, and triboelectric effects. For flex sensing with the impedance change of PAN-C/BTO nanofiber films during bending, it had a sensitivity of 1.12 deg^{-1} from 58.9° to 120.2° and a working range of 28°−150°. For self-powered force sensing, it had a gauge factor of 1.44 V·N^{-1} within the range of 0.15−25 N. The sensor had a long stability over 60 000 cycles at both sensing modes. The inclusion of barium titanate nanoparticles (BTO NPs) into the nanofiber film had an over 2.4 times enhancement of sensitivity for pressure sensing because of the synergy of piezoelectric and triboelectric effects. On the basis of multifunction and modularity, a series of potential applications of the sensor were demonstrated, including sensing human's swallowing, walking gaits, finger flexure, and finger-tapping. The self-powered flexible dual-mode sensor has great application potential in human-computer interactive and smart wearable sensing systems.

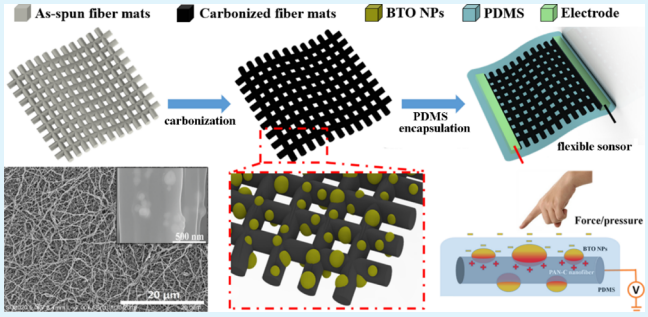

KEYWORDS: *self-powered, electrospinning, triboelectric nanogenerator, piezoelectric effect, flexible sensor*

1. INTRODUCTION

In recent years, flexible and wearable electronics have attracted great interests with their miniaturization, portability, and potential applications in the human−machine interface (HMI) and internet of things. Especially, several branches of flexible electronics, such as E-skin,[1,2] wearable sensors,[3,4] and wearable energy harvesting/storage device,[5−7] have obtained considerable development. As basic devices, flexible sensors play an important role in detecting substances in the environment and the changes of physical quantities and extending the sensory scope of human. Diverse flexible sensors have been proposed to detect heat,[8] force,[9] strain,[10] chemicals,[11] and so forth. The human physical indicators detected by flexible sensors include heart/pulse beating,[12] eyes blinking,[13] limbs bending,[10] and so forth. A certain sensor often detects one certain physical change and collects the signals to further help people to control the physical change in turn and thus achieves the interaction between human and machines.

Many kinds of flexible force sensors derived from different materials, such as metal nanowires,[14,15] carbon nanotube- or graphene-based materials,[4,16] and porous foam conducting materials,[17] have been proposed. The working mechanisms of the flexible force sensors are mainly based on resistive,[15,18] piezoelectric,[19,20] and capacitive effects.[4,14] More recently, self-powered flexible and wearable sensors based on a triboelectric nanogenerator (TENG) have become a research hotpot with the advantages of self-power, broad material selection, various structure designs, high sensitivity, and diverse applications.[21−23] However, these sensors can often work on the basis of a single mechanism with limited detection parameter and detection sensitivity. For example, a traditional piezoresistive or piezoelectric sensor can only detect strain or pressure. To meet the requirements for different applications, the development of

Received: February 10, 2018
Accepted: April 17, 2018
Published: April 17, 2018

DOI: 10.1021/acsami.8b02564
ACS Appl. Mater. Interfaces 2018, 10, 15855−15863

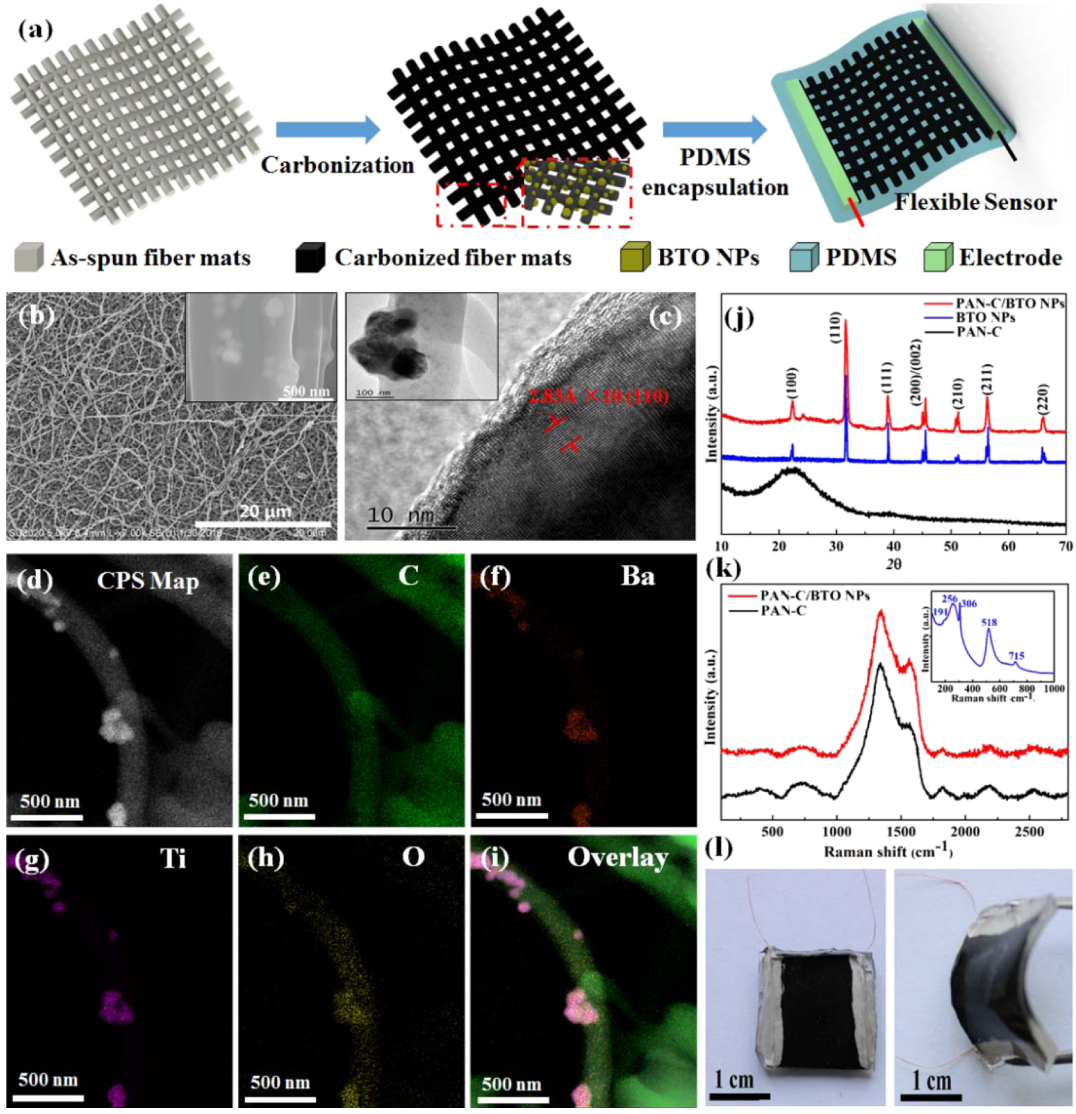

Figure 1. Flexible multifunctional PAN-C/BTO sensor. (a) Illustration showing the fabrication process of the PAN-C/BTO-based sensor. (b) SEM image of carbonized PAN/BTO nanofibers. (c) TEM image of carbonized PAN/BTO nanofibers. (d–i) EDX images of a single carbonized PAN-C/BTO nanofiber. (j) XRD curves of PAN-C, PAN-C/BTO nanofiber films, and BTO NPs. (k) Raman spectra of PAN-C and PAN-C/BTO nanofiber films; the inset shows the BTO NPs. (l) Photograph of a flexible dual-function PAN-C/BTO-based sensor.

multipurpose sensors with the ability to sensitively detect multiple parameters is urgently desired. A few research studies are only been reported very recently. For instance, Wang's group has built a self-powered pressure sensing system integrating the resistive sensor and TENG sensor.[24] Wang et al. proposed a dual-mode tactile sensor working in the piezoresistive sensory mode and self-powered TENG sensory mode.[17] Lee's group developed a dual-mode amenity force/humidity sensor based on the water–air TENG by characterizing two independent charge transfers.[25]

In this study, we have fabricated a multifunctional flexible sensor that can detect pressure and curvature independently and simultaneously by the integration of piezoelectric, triboelectric, and piezoresistive effects together. Fabricated by a convenient electrospinning, carbonization, and encapsulation process, the carbonized polyacrylonitrile/$BaTiO_3$ (PAN-C/BTO) nanofiber-based sensor can detect curvature based on the resistive mode and pressure based on the single-electrode TENG (SE-TENG) mechanism independently. With BTO NPs integrated into the carbonized PAN nanofibers, the output voltage and current of the flexible PAN-C/BTO-based sensor were greatly enhanced when working as a force sensor at a SE-TENG mode. As the first flexible dual-function sensor innovatively integrating the curvature measurement with pressure force sensing, the PAN-C/BTO nanofiber-based sensor was applied for human gesture capture, physical detection, and motion sensing. It has potential applications in the intelligent sensing system and HMI technology.

2. EXPERIMENTAL SECTION

2.1. Preparation of PAN/BTO Nanofiber Films. PAN (0.4 g, M_w = 15 000, Macklin) and $BaTiO_3$ nanoparticles (BTO NPs, 0.1 g, Sigma-Aldrich) were added into 3.6 g of *N*,*N*-dimethyl formamide (99.8%, AcroSeal). The mixture was ultrasonicated for 2 h after 1 h magnetic stirring and then poured into a 10 mL syringe for electrospinning. The laboratory-build electrospinning setup has a plate collector that was 15 cm away from the 25 G needle. A 15 kV high voltage was applied between the syringe needle and the collector. The electrospinning process was carried out at 25 °C, 30% relative humidity, and 1 mL/h injection rate. The as-spun PAN/BTO nanofiber films were dry for 4 h at 60 °C to volatilize the residual

DOI: 10.1021/acsami.8b02564
ACS Appl. Mater. Interfaces 2018, 10, 15855–15863

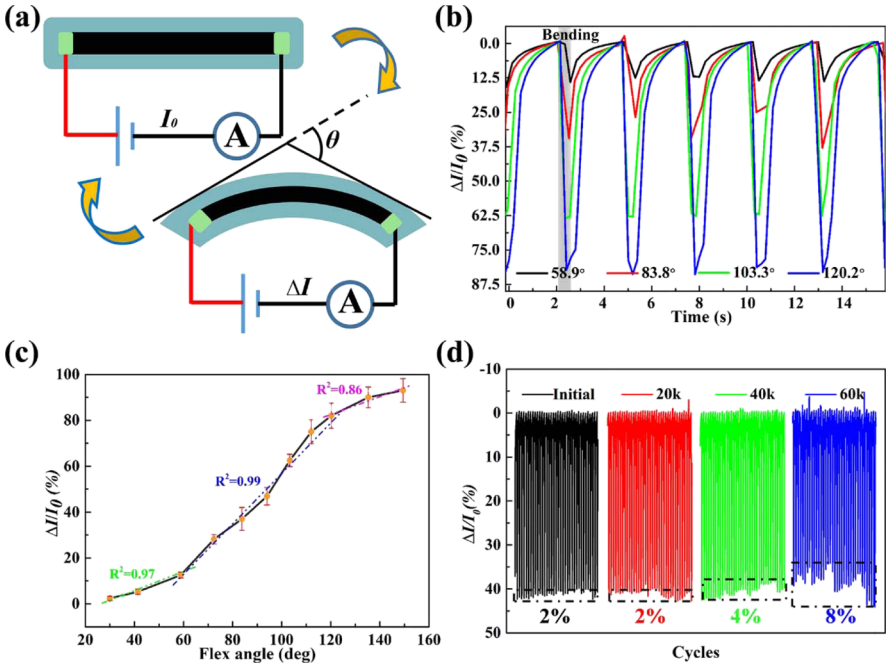

Figure 2. Electromechanical properties of the PAN-C/BTO-based sensor working as a flex sensor at the resistance mode. (a) Working schematic diagram of the PAN-C/BTO-based sensor working as a flex sensor. (b) Curves of relative change in current when the flex sensor working at 58.9°, 83.8°, 103.3°, and 120.2° of flex angles. (c) Relative change in current of the flex sensor vs the flex angle. (d) Relative change in current under repeated bending and releasing of 90° for 60 000 cycles, showing the durability of the sensor. The changes of $\Delta I/I_0$ were within 2% after 20 000 bending−releasing cycles, 4% after 40 000 cycles, and 8% after 60 000 cycles.

solvent. For PAN nanofiber films, electrospinning was performed without the addition of BTO NPs.

2.2. Fabrication of the Flexible Dual-Function Sensor. The PAN/BTO nanofiber films were heated in a tube furnace from room temperature (RT) to 240 °C with a heating rate of 5 °C min^{-1} and stabilized at 240 °C for 4 h in the ambient air. Then, the furnace was perfused with protective gas of argon, and the temperature was increased to 700 °C with a rate of 2 °C min^{-1} and kept for 1 h to carbonize the nanofiber films. During the course of temperature cooling to RT, the argon atmosphere was maintained. The carbonized PAN-C/BTO nanofiber films were cut into rectangular strips (1.5 cm × 1.5 cm) and connected to copper leads at two counter ends with silver paste. It was put on polydimethylsiloxane (PDMS, fabricated with a 10:1 mixture of base and curing agents, Dow Corning Sylgard 184) thin film (2 cm × 2 cm in size; 1 mm thick), and then liquid PDMS was smoothly covered onto the surface to encapsulate the device. Finally, the samples were cured at 80 °C for 3 h. The final sensors had a size of 2 cm × 2 cm and a thickness of ∼2 mm.

2.3. Characterizations and Performances. The morphology and structure of the nanofiber films were characterized by a field emission scanning electron microscope (Hitachi, SU-8020) and a high-resolution transmission electron microscope (TEM, Tecnai G2). X-ray diffraction (XRD) patterns were carried out by a PANalytical X'pert^3 powder diffractometer using a Cu Kα source with a step size of 0.013° and recorded over an angular range from 10° to 80°. Raman spectra were performed on a Raman spectroscope (HORIBA HR800) with a laser excitation wavelength of 532 nm. The bending deformation of the sensor was performed with a linear motor (Linmot), and the electrical signals of the strain were recorded at the same time by a Keithley 2400 digital meter at a constant voltage of 5 V. The pressure force applied on the sensor was monitored by a commercial sensor (501F01, YMC Piezotronics INC) mounted on the motion part of the linear motor, whereas the triboelectric output of the self-powered sensor was recorded by a Keithley 6514 electrometer.

3. RESULTS AND DISCUSSION

Electrospinning is a facile and convenient technique to produce nanofibers, especially for polymer materials. Importantly, inorganic NPs with special physicochemical properties could be incorporated to form composite nanofibers by choosing a suitable solvent to solve the polymer molecules and disperse the inorganic NPs concurrently. Figure 1a shows the fabrication process of the dual-functional PAN-C/BTO-based sensors. The PAN/BTO nanofibers were electrospun from the PAN solution mixed with BTO NPs and then carbonized under Ar atmosphere to endow them with good conductivity. The sensors were obtained by PDMS encapsulation of the PAN-C/BTO nanofiber film connected with copper wires at two terminals. Herein, randomly aligned nanofibers were fabricated using a flat plate collector, ensuring the generation of many mesoscopic joints with enhanced mechanical robustness. It was not as vulnerable as the oriented one that tended to be tore apart along the alignment direction.[26] From the scanning electron microscopy (SEM) image, the as-spun PAN/BTO nanofiber films had a randomly oriented structure with a nanofiber diameter of ∼400 nm (Figure S1 in the Supporting Information). Although protrusions could be observed, the as-spun nanofibers had a smooth surface and straight shape and had no conglutination between each other. After 700 °C treatment in the argon protection environment, the PAN nanofibers were carbonized (PAN-C/BTO). The whole nanofiber films turned into black from as-spun white, and the overall dimension was reduced (Figure S2 in the Supporting Information). The carbonated PAN-C/BTO nanofiber had a rough surface and many protrusions on the fiber surface. Especially, nanofibers were joined together at crisscross and overlaps, becoming curlier-like twisted roots (Figure 1b). The diameter of the nanofiber became uneven after carbonization. The overall mean diameter was ∼160 nm, much less than that

DOI: 10.1021/acsami.8b02564
ACS Appl. Mater. Interfaces 2018, 10, 15855−15863

before carbonization. The protrusions were caused by the heterogeneous distribution of BTO NPs during the formation of nanofibers (Figure 1b inset). Furthermore, a single PAN-C/BTO nanofiber was observed by TEM to discern the precise nanostructure (Figure 1c and inset). BTO NPs had a lattice fringe d_{110} = 2.8 Å, consistent with the crystal structure of original tetragonal BTO NPs (Figure S3 in the Supporting Information). They were aggregated to form a protrusion on the surface of the amorphous nanofiber.[27] Actually, the aggregation of BTO NPs was conducive to enhance the piezoelectric output power generation because the protrusions had a larger volume to effectively harvest an external applied mechanical stress and increase the total dipole moment.[28] Energy-dispersive X-ray spectroscopy reveals that BTO NPs (elements of Ba and Ti) were embedded in the carbonized nanofiber (Figure 1d–i). It was worth noting that O existed not only in BTO NPs but also in the carbonized nanofiber, which was caused by the oxidation of carbon fiber in the air at 240 °C.

The XRD spectrum also proved that the PAN-C nanofiber had an amorphous structure with a carbon peak centered at 23° (Figure 1j). PAN-C/BTO nanofibers had characteristic peaks corresponding to the (100), (110), (111), (200), (210), (211), and (220) planes of crystalline BTO, identical to free BTO NPs.[29−32] It is noteworthy that the peak splitting at 45° for (200) and (002) planes indicated that the BTO NPs had a tetragonal phase with a piezoelectric effect (Figure 1j).[33,34] PAN-C nanofibers (carbonized PAN nanofibers without BTO NPs) and PAN-C/BTO nanofibers showed similar Raman spectrum patterns with peaks at 1360 cm^{-1} [defects or heteroatom doping (D-band)], and 1580 cm^{-1} [crystalline sp^2 carbon (G-band)] (Figure 1k).[35] The D-band peak was higher than the G-band peak, indicating that the nanofiber films had a defective or heteroatom-doped graphene structure. The I_d/I_g value of the PAN-C/BTO nanofibers was about 1.9. For PAN-based carbonized nanofibers, the conductivity was reported to increase with the pyrolysis temperature and also increased considerably with the pyrolysis time at lower pyrolysis temperature.[36,37] No peaks corresponding to tetragonal BTO (Figure 1k inset) was observed for PAN-C/BTO nanofibers, which may be attributed to the low percentage of BTO NPs. If we analyze the Raman spectrum of BTO NPs solely, the characteristic peaks of the tetragonal phase could be observed in the range of 100−1000 cm^{-1} (Figure 2f inset). The peaks at 191 cm^{-1} [A_1(TO), E(LO)], 256 cm^{-1} [A_1(TO)], 306 cm^{-1}[B_1, E(TO + LO)], 518 cm^{-1} [E, A_1(TO)], and 715 cm^{-1} [A_1, E(LO)] were all subjective to the tetragonal phase of BTO NPs.[27,28]

The two terminals of the carbonized nanofiber films were connected with copper wires by silver paste and encapsulated by PDMS (Figure 1l). PDMS is a kind of low-cost, simple-to-use, chemically inert polymer. In view of the flexibility and biocompatibility of cured PDMS, it has been extensively applied in wearable electronic devices.[22,38,39] The final device had a size of 2 × 2 cm and a thickness of 2 mm with good flexibility (Figure 1l). Because of the PDMS encapsulation, the PAN-C/BTO-based sensor was waterproof. After being immersed in water for 10 min, the output signal of the dried sensor was not affected (Figure S4 in the Supporting Information).

The flexible sensor based on PDMS-encapsulated PAN-C/BTO could work for the detection of motions including bending and pressing. The schematic of testing setup is shown in Figure S5 in the Supporting Information. The flex sensor was bended when the force was applied on its both ends, and the bending degree could be defined by the flex angle (Figure 2a). In our experiment, the bending of the flex sensor was performed by pushing inward the two free ends of the sensor (Figure S5). The sensing principle was based on the impedance change of the conducting nanofiber film. The bending deformation of the sensor led to the bend and stretch of the conducting nanofiber film, thus increasing the resistance. When the deformation was recovered, the conducting fiber layer returned to its initial state and the resistance came back to the unbending state. It was noteworthy that the conductivity of the PAN-C/BTO nanofiber film was comparable (~10.25 kΩ sq^{-1}) to that of the PAN-C nanofiber film (~6.54 kΩ sq^{-1}). Because of the flexible encapsulating material, a conducting nanofiber layer was supported and restricted during bending deformation so that it would not be broken. Similar to the resistive strain gauges, here, we defined the gauge factor (GF) as the relative change in current divided by the flex angle

$$\mathrm{GF} = \frac{\Delta I}{I_0 \theta} \tag{1}$$

$$\Delta I = |I - I_0| \tag{2}$$

where I is the real-time current of the sensor with bending, and I_0 is the current of the sensor without bending, and θ is the flex angle. ΔI is the absolute value of the difference between current at bending and releasing. Figure 2b is a real-time measurement of the relative change of current ($\Delta I/I_0$) under a series of flex angles at 58.9°, 83.8°, 103.3°, and 120.2° for the PAN-C/BTO-based flex sensor. In comparison, the real-time $\Delta I/I_0$ curves of the PAN-C-based flex sensor at the same bending angles are shown in Figure S6. The PAN-C-based flex sensor had a signal strength similar to that of the PAN-C/BTO-based one, indicating that doping of BTO NPs did not affect the sensitivity of the flex sensor. The relationship between $\Delta I/I_0$ and angle magnitude is plotted in Figure 4c. When the flex angle of the sensor increased from 28° to 150°, $\Delta I/I_0$ significantly increased from 2% to 92%, along with the resistance increase of the conducting nanofiber layer. The GFs of the flex sensor were calculated, by separating the flex angle into three angle ranges and fitting the curve, to be 0.36 deg^{-1} from 30° to 58.9°, 1.12 deg^{-1} from 58.9° to 120.2°, and 0.37 deg^{-1} from 120.2° to 149.4°. To further demonstrate the stability of the flex sensor, a continuous bending cycle of 90° was applied to the sensor. The sensor maintained a high signal-to-noise ratio, and the changes of $\Delta I/I_0$ were within 2% after 20 000 bending−releasing cycles, 4% after 40 000 cycles, and 8% after 60 000 cycles (Figure 2d). The fluctuation could be attributed to the slight fatigue wear. Furthermore, as a flex sensor, it could also detect the applied force during bending. In the bending−releasing process, a horizontal impulse force was applied onto the sensor at bending and releasing status. Because the horizontal impulse force affected the curvature of the sensor, new peaks could be distinguished in both bending and releasing signal curves (Figure S7 in the Supporting Information). At the extreme position of bending, a small reverse peak appeared at the original signal peak maximum. It was because the horizon force impeded bending, inducing a ~5% $\Delta I/I_0$ signal degradation. At the releasing status, the horizon force caused slight bending, so a small peak appeared, which represented an 8% $\Delta I/I_0$ signal generation. It suggested that the flexible sensor could achieve a sensitive tactile detection during curvature sensing.

DOI: 10.1021/acsami.8b02564
ACS Appl. Mater. Interfaces 2018, 10, 15855−15863

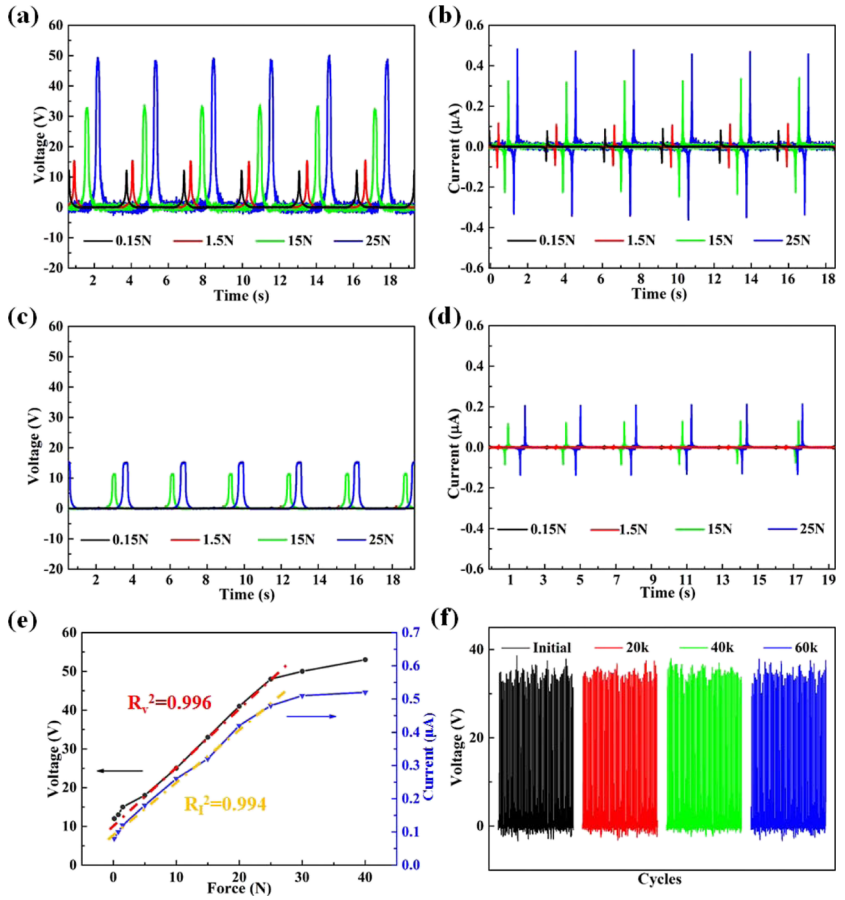

Figure 3. PAN-C/BTO-based sensor and PAN-C-based sensor working as a self-powered pressure sensor at the triboelectric mode. The open-circuit voltage (a) and short-circuit current (b) of the PAN-C/BTO-based pressure sensor. The open-circuit voltage (c) and short-circuit current (d) of the PAN-C-based pressure sensor. They show that the PAN-C/BTO-based pressure sensor has a higher V_{oc} and I_{sc} signal than those of the PAN-C-based pressure sensor. (e) Open-circuit voltage and short-circuit current of the PAN-C/BTO self-powered pressure sensor under different pressure forces. (f) Voltage signal under repeated loading and unloading of a 15 N impulse force for 60 000 cycles, showing the durability of the self-powered pressure sensor.

As a dual-function flexible sensor, it can not only detect bending angle in a large range but also work for self-powered pressure sensing. When the sensor worked for pressure sensing, it was in essence as a SE-TENG. The flexible encapsulating material of PDMS worked as a dielectric layer to produce an electrical charge by the contact electrification, and the carbonized nanofiber layer acted as an electrode to collect those charges and conduct current. In the measurement process, a piece of clean and smooth Kapton film (Φ11.5 mm) was stuck on a commercial force sensor as the active part to contact with the PAN-C/BTO sensor. The commercial force sensor had an 11.5 mm diameter with the end face as the stress surface, so the contact area of the forcing punch has a Φ11.5 mm circular area. As previously mentioned, the flexible sensor had a 2 × 2 cm rectangular PDMS surface. The self-leveling PDMS had a smooth and clean surface after curing. The schematic of measurement setup for the self-powered force sensor is shown in Figure S5. An impulse force was applied onto the sensor surface to measure the actual force by a linear motor. Two independent sensors were measured, one with PAN-C/BTO NP nanofiber and the second of PAN-C nanofiber without BTO NPs. The real-time measurement result of open-circuit voltage (V_{oc}) and short-circuit current (I_{sc}) of the PAN-C/BTO-based sensor under various pressures is shown in Figure 3a,b, respectively. The PAN-C/BTO-based sensor had V_{oc}/I_{sc} electric outputs of 12 V/0.08 μA, 15 V/0.11 μA, 32 V/0.32 μA, and 49 V/0.48 μA under 0.15, 1.5, 15, and 25 N impulse force, respectively. Compared to the PAN-C/BTO-based sensor, the PAN-C-based sensor had a lower electric output under the same pressure (2.7−12 times lower in V_{oc} and 2.3−13 times lower in I_{sc} under different pressures). Its V_{oc} values were 1, 2, 12, and 15 V, whereas I_{sc} values were 6, 13, 120, and 205 nA under 0.15, 1.5, 15, and 25 N impulse force, respectively (Figure 3c,d). It was speculated that remarkable signal enhancement of the PAN-C/BTO-based sensor was owing to the piezoelectric effect of BTO NPs embedded in the carbonized nanofiber. The relationship between V_{oc}, I_{sc}, and magnitude of angle is plotted in Figure 3e. There was a favorable linear relationship between the electric output (R_V^2 = 0.996 for V_{oc} or R_I^2 = 0.994 for I_{sc}) and force from 0.15 to 25 N, indicating that the PAN-C/BTO-based sensor was reliable for force detecting. The triboelectric outputs increased with the increase of pressure, which may be attributed to the largened contact area. When a rigid counterpart material was pressed on the soft PDMS with increased pressure, the contact area would also increase because of the microcosmic deformation of PDMS. When the pressure increased to a certain extent, PDMS was compressed to a threshold and the contact area would not increase anymore. Therefore, the triboelectric outputs had no significant increase when the pressure was higher than 25 N.

DOI: 10.1021/acsami.8b02564
ACS Appl. Mater. Interfaces 2018, 10, 15855−15863

Similarly, the sensitivity of the force sensor is defined by the equation of

$$GF = \frac{V_{oc}}{F} \quad (3)$$

where V_{oc} is the open-circuit voltage when the pressure is applied on the sensor and F is the applied pressure. The calculated GF of the force sensor was 1.44 $V \cdot N^{-1}$ within the range of 0.15−25 N. As a SE-TENG, its triboelectric output is largely dependent on the opposite material. In different usage environments, the triboelectric output would be affected by temperature, humidity, and surface properties of opposite material. Therefore, before using the PAN-C/BTO-based sensor to accurately measure force, calibration should be performed in advance.

As a pressure sensor, the PAN-C/BTO sensor is commonly put on a flat surface, which would not bend under pressure. In some circumstances, the sensor may bend while applying force. To simulate, the two terminal ends of the sensor were supported by two stands, allowing the sensor to bend under pressure (Figure S8). From the real-time V_{oc} curves of the sensor under pressure with bending and without bending, the V_{oc} of the bent sensor under pressure was slightly lower than that without bending because the sensor could not sufficiently contact with the counterpart. Furthermore, the peak of the bent sensor oscillated at the high voltage value for longer time because of the longer contact time during the bending deformation of the sensor. The PAN-C/BTO-based sensor also had an extraordinary stability when working at the TENG mode. The triboelectric output had no obvious change after 60 000 pressure loading−unloading cycles (Figure 3f).

The tetragonal barium titanium nanocrystal has a crystal structure with one body-centered Ti atom, six face-centered O atoms, and eight Ba atoms at each corner (Figure 4a). When BTO is subjected to a mechanical stress, it is poled by structural deformation to generate a local piezoelectric potential. The PAN-C/BTO-based flexible sensor is composed of three functional components: carbonized PAN nanofibers as the electrode, BTO NPs embedded in the nanofibers for providing the piezoelectric effect, and the encapsulating PDMS as the friction layer (Figure 4b). PDMS is a kind of commonly used flexible triboelectric material, and it is negative in triboelectric series.[40] When an active object, such as human hand, contacts with PDMS, triboelectrification occurs at the interface. Simultaneously, the stress caused by the contact makes BTO deform to generate a local piezoelectric potential, enhancing the surface potential of the sensor (Figure 4c). When the object departs away from the surface of the sensor, an equivalent positive charge would be induced on the conductive PAN-C/BTO nanofiber layer because of the electrostatic induction effect (Figure 4d). This process accompanies with the charge flowing. Until the active object is far away from the sensor, the electron flowing stops (Figure 4e). As the active object approaches the sensor again, electrons would flow from the ground to the PAN-C/BTO nanofiber layer (Figure 4f). Then, the next cycle starts from contacting between the object and the sensor (Figure 4c).

The effect of the BTO NPs on the output performance was investigated as well. In our study, BTO can enhance the output performance of the self-powered pressure sensor (Figure 5a,b). The direction of the piezoelectric polarization of BTO NPs in this system is perpendicular to the axis of PAN-C. To verify this mechanism, the potential distribution of the PAN-C/BTO

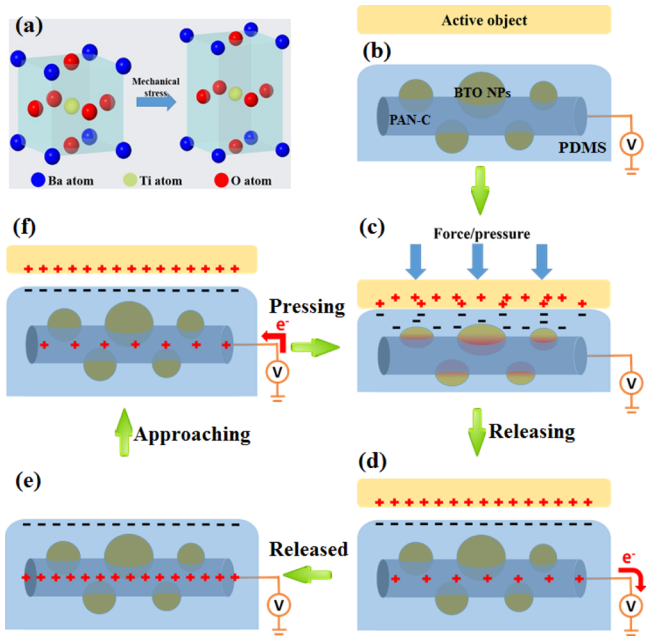

Figure 4. Working mechanism of the PAN-C/BTO-based self-powered pressure sensor. (a) BTO NPs are poled to create a piezoelectric potential when a mechanical force is applied onto the sensor. (b) Original state of the sensor before contacting with an active object. (c) Moment of contacting and pressing between the object and the sensor. (d) Active object starts to depart from the sensor, and the pressure has been released. (e) Active object is far away from the sensor. (f) Active object is approaching the sensor and preparing to press on the sensor.

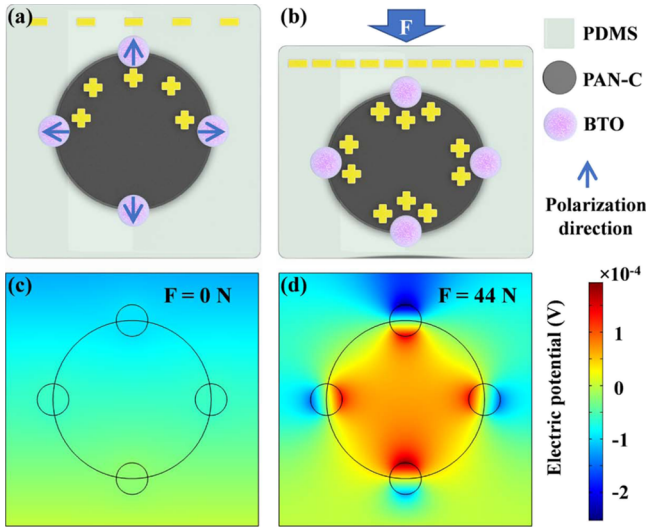

Figure 5. Working mechanism of BTO NPs enhancing the output performance. (a,b) Schematic diagram of the self-powered pressure sensor with $F = 0$ and $F = Fx$. (c,d) Finite-element simulation of the potential distribution of the PAN-C/BTO nanofiber layer.

nanofiber layer was analyzed by finite-element simulation with the commercial software COMSOL (Figure 5c,d). Simulation studies have shown that when the force is applied, the output performance is enhanced because of the piezoelectric effect on the BTO NPs. As the force increases, the negative charge on the surface and the positive charge in PAN-C increase accordingly (Supporting Information Video 1). This mecha-

DOI: 10.1021/acsami.8b02564
ACS Appl. Mater. Interfaces 2018, 10, 15855−15863

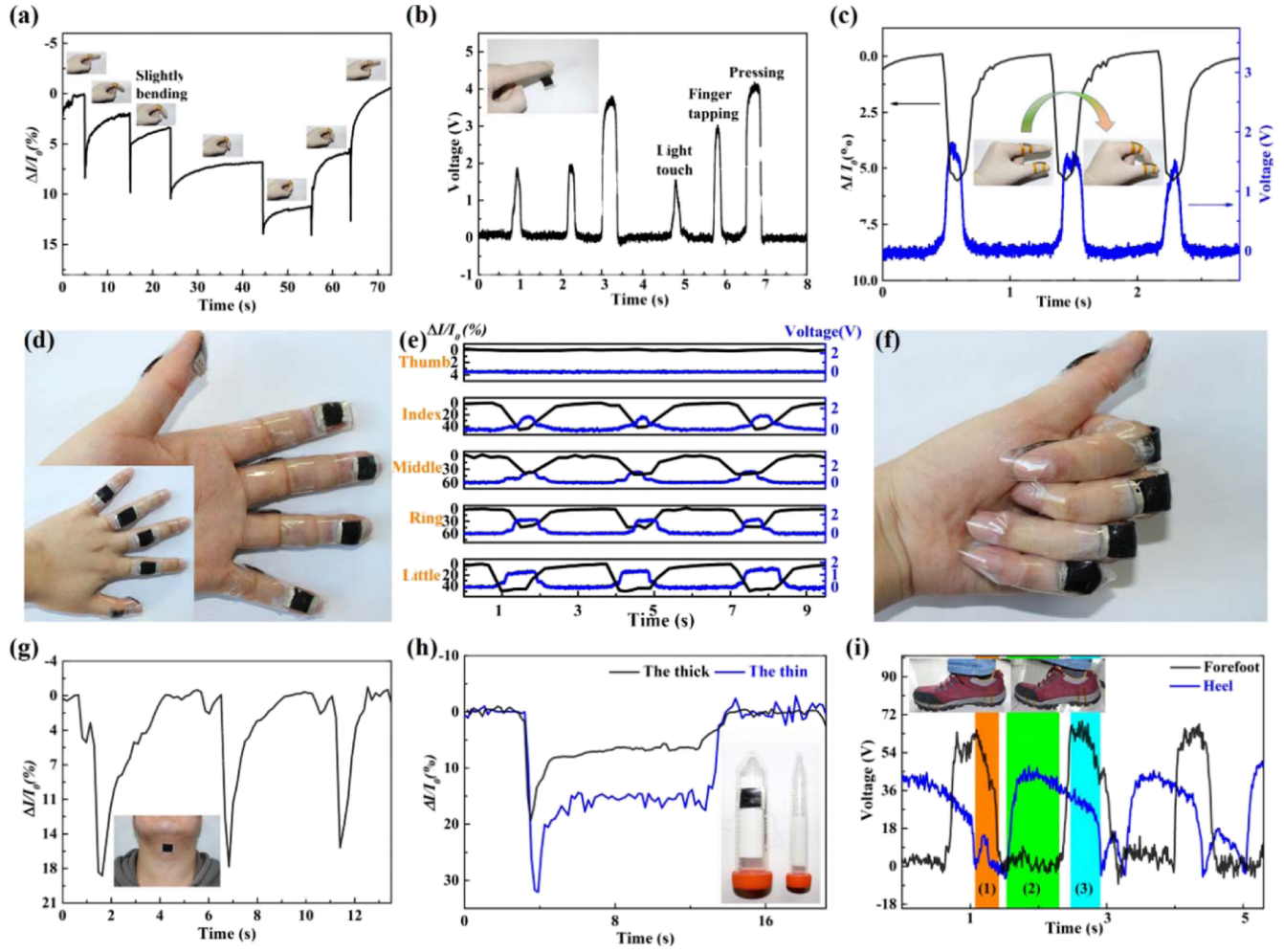

Figure 6. Detection of different human motions and flexural measurement using the flexible dual-function PAN-C/BTO-based sensor. (a) When the sensor was attached on the knuckle, it can detect different bending degrees of the finger knuckle. (b) As a self-powered tactile sensor, it can sense different contact strengths. (c) By combining the two working modes, the sensor on the knuckle (flex sensing mode) and on the fingertip (self-powered pressure sensing mode) could express a pinching motion. (d) Smart sensing system was proposed with integrating two sensors on each finger. It could express different hand gesture, such as (e) finger spray for (f) a "good" gesture. (g) Sensor can detect action of swallowing. (h) Flex sensor can measure the thickness of cylinders during the process of bending onto them because of different curvature radii. (i) When two PAN-C/BTO-based self-powered pressure sensors were attached under a shoe, they could detect human walking synergistically. (1) The heel is touching the ground with the forefoot falling. (2) The heel is lifting and the forefoot remains in contact with the ground. (3) The foot has left the floor.

nism optimizes the output performance by coupling triboelectric charges and piezoelectric charges.

Owing to the outstanding flexibility and versatility, the PAN-C/BTO-based sensor has promising applications in wearable devices. Attached on the knuckle of a volunteer, the PAN-C/BTO-based flex sensor could be used to capture the subtle motions of human fingers. Figure 6a shows a whole bending−extending cycle curve of a finger-free movement. In the bending process, a slight bending could be detected sensitively (Supporting Information Video 2). In addition to the common bending activities, the finger touch is another important finger activity. With a self-powered force sensing ability, the PAN-C/BTO-based sensor could distinguish different strength of touches (Supporting Information Video 3). By measuring the open-circuit voltage between the sensor and the ground, the PAN-C/BTO-based sensor could sense the strength of finger touch without any external power supply. The PAN-C/BTO-based sensor could recognize the light touch, finger tapping, and pressing easily (Figure 6b). On the basis of its multifunction, one sensor was attached on the finger joint to sense the bending motion and another was stuck on the finger pulp to detect the touch movement, simultaneously. A "pinching" gesture could be captured (Figure 6c). The sensor with good modularity could be conveniently integrated into a sensing system. For example, a gesture sensing system composed of 10 sensors (Figure 6d). Figure 6e shows the curves of fingers' bending−stretching movements, which expressed a "good" gesture language in Figure 6f. $\Delta I/I_0$ curves originated from the signals of the fingers bending (from sensors on the knuckle back), and voltage curves are signals of finger pulps contacting with palm (from sensors on the finger pads). There is no $\Delta I/I_0$ or voltage signal from the thumb because it was not moved during the course of action. Therefore, two sensors on different positions of one finger could detect the movements of the finger independently, and several modularized sensors could sense more complicated motions synergistically.

As a compact and portable wearable sensor, it can also monitor human health-related motion such as swallowing (Figure 6g). When swallowing, the larynx is raised and pressed

DOI: 10.1021/acsami.8b02564
ACS Appl. Mater. Interfaces 2018, 10, 15855−15863

forward and the laryngeal passage is blocked to prevent the food entering the trachea.[41] During this process, laryngeal prominence moves up and down. The PAN-C/BTO-based sensor was stuck on the laryngeal prominence of a male volunteer. When swallowing, the sensor was bent with the laryngeal prominence lifting. The sensor totally detected three swallowing actions during 13 s. Therefore, the sensor had the potential in health monitoring to detect the eating process of a patient. The PAN-C/BTO-based sensor could also distinguish the material shape and geometry based on the bending action. By sticking the flex sensors onto the surface of two cylinders with different diameters, the flex sensor had different bending deformations to induce differentiated current signals (Figure 6h).

Figure 6i presents the real-time voltage change of two PAN-C/BTO-based sensors attached at the bottom of a shoe. One sensor was attached under the forefoot and another under the heel so that they could sense the human's gait. They could work as self-powered tactile sensors to detect the contact between the sole and the smooth marble floor. The marble floor with a smooth and clean surface could fully contact with the PDMS sensor. It was triboelectro-positive relative to PDMS. Generally, during human walking, the heel will touch the ground first with the forefoot falling and this process (1) is short in time. In process (2), the heel lifts and the forefoot remains in contact with the ground. Therefore, the sensor under the heel has a higher voltage signal, and the one under the forefoot maintains a low triboelectric potential. This process takes longer time because the other leg is moving forward when the forefoot remains on the ground. In process (3), the foot leaves the floor and both sensors have high triboelectric outputs. In this way, the PAN-C/BTO-based sensors detected a complete process of one step from foot falling down to lifting the ground. If more sensors are integrated under soles to form a sensing system, they can detect the gait of different people because of the different plantar force distributions. Therefore, the sensor is expected to use as a multifunctional sensor for human health monitoring.

4. CONCLUSIONS

In summary, we have fabricated a wearable and flexible sensor via a facile electrospinning, carbonization, and encapsulation process. On the basis of the integration of piezoresistive, triboelectric, and piezoelectric effects, it had the advantages of multifunction, modularization, and high sensitivity. For flexural sensing, the PAN-C/BTO-based sensor had a GF of 1.12 deg^{-1} from 58.9° to 120.2° and a working range of 28°−150°. For self-powered force sensing, it had a high sensitivity of 1.44 $V \cdot N^{-1}$ in the range of 0.15−25 N. Furthermore, the PAN-C/BTO-based sensor had a high stability (>60 000 cycles) when working as either a flex sensor or a force sensor. According to the finite-element model, the high signal strength of the self-powered force senor was originated from the triboelectric output and piezoelectric output of the BTO NPs. The sensors could be used for bending and tactile sensing and be assembled into a gesture sensing system based on their modularity. As a medical monitoring sensor, it could be used to monitor swallowing motion of human or perform basic bending measurement. These sensors could also be integrated into soles to capture the human gait. On the basis of the numerous advantages, the PAN-C/BTO-based sensor has broad application prospects in future wearable electronics.

ASSOCIATED CONTENT

Supporting Information

The Supporting Information is available free of charge on the ACS Publications website at DOI: 10.1021/acsami.8b02564.

SEM image of as-spun PAN/BTO nanofibers; photos of electrospun nanofiber film before and after carbonization; TEM image of BTO NPs; waterproof of the PAN-C/BTO-based flex sensor; real-time $\Delta I/I_0$ curves of PAN-C-based flex sensor; real-time $\Delta I/I_0$ curves of PAN-C-based flex sensor subjected to a horizontal impulse force; and real-time V_{oc} curves of the sensor with/without bending under pressure (PDF)

Dynamic change process of potential on the sensor surface during applying pressure (AVI)

Sensing of finger bending (AVI)

Self-powered force sensing (AVI)

AUTHOR INFORMATION

Corresponding Authors

*E-mail: zhangyan@uestc.edu.cn. Phone: +86-28-83200098 (Y.Z.).

*E-mail: lilinlin@binn.cas.cn. Phone: +86-10-82854770. Fax: +86-140-82854800 (L.L).

ORCID

Lijie Li: 0000-0003-4630-7692

Caofeng Pan: 0000-0001-6327-9692

Yan Zhang: 0000-0002-7329-0382

Linlin Li: 0000-0003-1041-4533

Notes

The authors declare no competing financial interest.

ACKNOWLEDGMENTS

The work was supported by the National Natural Science Foundation of China (no. 81471784), Nature Science Foundation of Beijing (2172058), the Youth Innovation Promotion Association of the Chinese Academy of Sciences (2015023), and the "Thousands Talents" program for pioneer researcher and his innovation team, China.

REFERENCES

(1) Chortos, A.; Liu, J.; Bao, Z. Pursuing Prosthetic Electronic Skin. *Nat. Mater.* **2016**, *15*, 937−950.

(2) Chou, H.-H.; Nguyen, A.; Chortos, A.; To, J. W. F.; Lu, C.; Mei, J.; Kurosawa, T.; Bae, W.-G.; Tok, J. B.-H.; Bao, Z. A Chameleon-Inspired Stretchable Electronic Skin with Interactive Colour Changing Controlled by Tactile Sensing. *Nat. Commun.* **2015**, *6*, 8011.

(3) Lee, S.; Reuveny, A.; Reeder, J.; Lee, S.; Jin, H.; Liu, Q.; Yokota, T.; Sekitani, T.; Isoyama, T.; Abe, Y.; Suo, Z.; Someya, T. A Transparent Bending-Insensitive Pressure Sensor. *Nat. Nanotechnol.* **2016**, *11*, 472−478.

(4) Lipomi, D. J.; Vosgueritchian, M.; Tee, B. C.-K.; Hellstrom, S. L.; Lee, J. A.; Fox, C. H.; Bao, Z. Skin-like Pressure and Strain Sensors Based on Transparent Elastic Films of Carbon Nanotubes. *Nat. Nanotechnol.* **2011**, *6*, 788−792.

(5) Wang, J.; Li, S.; Yi, F.; Zi, Y.; Lin, J.; Wang, X.; Xu, Y.; Wang, Z. L. Sustainably Powering Wearable Electronics Solely by Biomechanical Energy. *Nat. Commun.* **2016**, *7*, 12744.

(6) Chen, J.; Huang, Y.; Zhang, N.; Zou, H.; Liu, R.; Tao, C.; Fan, X.; Wang, Z. L. Micro-cable Structured Textile for Simultaneously Harvesting Solar and Mechanical Energy. *Nat. Energy* **2016**, *1*, 16138.

(7) Gao, Y.; Gu, J.; Li, L.; Zhao, W.; Li, Y. Synthesis of Gold Nanoshells Through Improved Seed-mediated Growth Approach: Brust-like, In Situ Seed Formation. *Langmuir* **2016**, *32*, 2251−2258.

DOI: 10.1021/acsami.8b02564
ACS Appl. Mater. Interfaces 2018, 10, 15855−15863

(8) Ren, X.; Pei, K.; Peng, B.; Zhang, Z.; Wang, Z.; Wang, X.; Chan, P. K. L. A Low-Operating-Power and Flexible Active-Matrix Organic-Transistor Temperature-Sensor Array. *Adv. Mater.* **2016**, *28*, 4832−4838.
(9) Ma, Y.; Liu, N.; Li, L.; Hu, X.; Zou, Z.; Wang, J.; Luo, S.; Gao, Y. A Highly Flexible and Sensitive Piezoresistive Sensor Based on MXene with Greatly Changed Interlayer Distances. *Nat. Commun.* **2017**, *8*, 1207.
(10) Wang, C.; Li, X.; Gao, E.; Jian, M.; Xia, K.; Wang, Q.; Xu, Z.; Ren, T.; Zhang, Y. Carbonized Silk Fabric for Ultrastretchable, Highly Sensitive, and Wearable Strain Sensors. *Adv. Mater.* **2016**, *28*, 6640−6648.
(11) Khim, D.; Ryu, G.-S.; Park, W.-T.; Kim, H.; Lee, M.; Noh, Y.-Y. Precisely Controlled Ultrathin Conjugated Polymer Films for Large Area Transparent Transistors and Highly Sensitive Chemical Sensors. *Adv. Mater.* **2016**, *28*, 2752−2759.
(12) Li, Z.; Wang, Z. L. Air/Liquid-pressure and Heartbeat-Driven Flexible Fiber Nanogenerators as A Micro/Nano-Power Source or Diagnostic Sensor. *Adv. Mater.* **2011**, *23*, 84−89.
(13) Pu, X.; Guo, H.; Chen, J.; Wang, X.; Xi, Y.; Hu, C.; Wang, Z. L. Eye Motion Triggered Self-Powered Mechnosensational Communication System Using Triboelectric Nanogenerator. *Sci. Adv.* **2017**, *3*, No. e1700694.
(14) Yao, S.; Zhu, Y. Wearable Multifunctional Sensors Using Printed Stretchable Conductors Made of Silver Nanowires. *Nanoscale* **2014**, *6*, 2345−2352.
(15) Gong, S.; Schwalb, W.; Wang, Y.; Chen, Y.; Tang, Y.; Si, J.; Shirinzadeh, B.; Cheng, W. A Wearable and Highly Sensitive Pressure Sensor with Ultrathin Gold Nanowires. *Nat. Commun.* **2014**, *5*, 3132.
(16) Shin, S.-H.; Ji, S.; Choi, S.; Pyo, K.-H.; An, B. W.; Park, J.; Kim, J.; Kim, J.-Y.; Lee, K.-S.; Kwon, S.-Y.; Heo, J.; Park, B.-G.; Park, J.-U. Integrated Arrays of Air-Dielectric Graphene Transistors as Transparent Active-Matrix Pressure Sensors for Wide Pressure Ranges. *Nat. Commun.* **2017**, *8*, 14950.
(17) Wang, Z.; Jiang, R.; Li, G.; Chen, Y.; Tang, Z.; Wang, Y.; Liu, Z.; Jiang, H.; Zhi, C. Flexible Dual-mode Tactile Sensor Derived from Three-dimensional Porous Carbon Architecture. *ACS Appl. Mater. Interfaces* **2017**, *9*, 22685−22693.
(18) Gao, Y.; Ota, H.; Schaler, E. W.; Chen, K.; Zhao, A.; Gao, W.; Fahad, H. M.; Leng, Y.; Zheng, A.; Xiong, F.; Zhang, C.; Tai, L.-C.; Zhao, P.; Fearing, R. S.; Javey, A. Wearable Microfluidic Diaphragm Pressure Sensor for Health and Tactile Touch Monitoring. *Adv. Mater.* **2017**, *29*, 1701985.
(19) Park, D. Y.; Joe, D. J.; Kim, D. H.; Park, H.; Han, J. H.; Jeong, C. K.; Park, H.; Park, J. G.; Joung, B.; Lee, K. J. Self-Powered Real-Time Arterial Pulse Monitoring Using Ultrathin Epidermal Piezoelectric Sensors. *Adv. Mater.* **2017**, *29*, 1702308.
(20) Chen, Z.; Wang, Z.; Li, X.; Lin, Y.; Luo, N.; Long, M.; Zhao, N.; Xu, J.-B. Flexible Piezoelectric-Induced Pressure Sensors for Static Measurements Based on Nanowires/Graphene Heterostructures. *ACS Nano* **2017**, *11*, 4507−4513.
(21) Lin, Z.; Chen, J.; Li, X.; Zhou, Z.; Meng, K.; Wei, W.; Yang, J.; Wang, Z. L. Triboelectric Nanogenerator Enabled Body Sensor Network for Self-Powered Human Heart-Rate Monitoring. *ACS Nano* **2017**, *11*, 8830−8837.
(22) Seung, W.; Gupta, M. K.; Lee, K. Y.; Shin, K.-S.; Lee, J.-H.; Kim, T. Y.; Kim, S.; Lin, J.; Kim, J. H.; Kim, S.-W. Nanopatterned Textile-Based Wearable Triboelectric Nanogenerator. *ACS Nano* **2015**, *9*, 3501−3509.
(23) Guo, W.; Zhang, X.; Yu, X.; Shu, W.; Qiu, J.; Tang, W.; Li, L.; Liu, H.; Wang, Z. L. Self-Powered Electrical Stimulation for Enhancing Neural Differentiation of Mesenchymal Stem Cells on Graphene-Poly(3,4-ethylenedioxythiophene) Hybrid Microfibers. *ACS Nano* **2016**, *10*, 5086−5095.
(24) Luo, J.; Fan, F. R.; Zhou, T.; Tang, W.; Xue, F.; Wang, Z. L. Ultrasensitive Self-Powered Pressure Sensing System. *Extreme Mech. Lett.* **2015**, *2*, 28−36.
(25) Wang, H.; Wu, H.; Hasan, D.; He, T.; Shi, Q.; Lee, C. Self-Powered Dual-Mode Amenity Sensor Based on the Water−Air Triboelectric Nanogenerator. *ACS Nano* **2017**, *11*, 10337−10346.
(26) Zhang, C.-L.; Yu, S.-H. Nanoparticles Meet Electrospinning: Recent Advances and Future Prospects. *Chem. Soc. Rev.* **2014**, *43*, 4423−4448.
(27) Lin, Z.-H.; Yang, Y.; Wu, J. M.; Liu, Y.; Zhang, F.; Wang, Z. L. $BaTiO_3$ Nanotubes-Based Flexible and Transparent Nanogenerators. *J. Phys. Chem. Lett.* **2012**, *3*, 3599−3604.
(28) Shin, S.-H.; Kim, Y.-H.; Lee, M. H.; Jung, J.-Y.; Nah, J. Hemispherically Aggregated $BaTiO_3$ Nanoparticle Composite Thin Film for High-Performance Flexible Piezoelectric Nanogenerator. *ACS Nano* **2014**, *8*, 2766−2773.
(29) Alluri, N. R.; Chandrasekhar, A.; Vivekananthan, V.; Purusothaman, Y.; Selvarajan, S.; Jeong, J. H.; Kim, S.-J. Scavenging Biomechanical Energy Using High-Performance, Flexible $BaTiO_3$ Nanocube/PDMS Composite Films. *ACS Sustainable Chem. Eng.* **2017**, *5*, 4730−4738.
(30) Zhuang, Y.; Li, F.; Yang, G.; Xu, Z.; Li, J.; Fu, B.; Yang, Y.; Zhang, S. Fabrication and Piezoelectric Property of $BaTiO_3$ Nanofibers. *J. Am. Ceram. Soc.* **2014**, *97*, 2725−2730.
(31) Bowland, C. C.; Malakooti, M. H.; Sodano, H. A. Barium Titanate Film Interfaces for Hybrid Composite Energy Harvesters. *ACS Appl. Mater. Interfaces* **2017**, *9*, 4057−4065.
(32) Ávila, H. A.; Ramajo, L. A.; Góes, M. S.; Reboredo, M. M.; Castro, M. S.; Parra, R. Dielectric Behavior of Epoxy/$BaTiO_3$ Composites Using Nanostructured Ceramic Fibers Obtained by Electrospinning. *ACS Appl. Mater. Interfaces* **2013**, *5*, 505−510.
(33) Yan, J.; Jeong, Y. G. High Performance Flexible Piezoelectric Nanogenerators Based On $BaTiO_3$ Nanofibers in Different Alignment Modes. *ACS Appl. Mater. Interfaces* **2016**, *8*, 15700−15709.
(34) Mahadeva, S. K.; Walus, K.; Stoeber, B. Piezoelectric Paper Fabricated via Nanostructured Barium Titanate Functionalization of Wood Cellulose Fibers. *ACS Appl. Mater. Interfaces* **2014**, *6*, 7547−7553.
(35) Ferrari, A. C.; Robertson, J. Resonant Raman Spectroscopy of Disordered, Amorphous, and Diamondlike Carbon. *Phys. Rev. B: Condens. Matter Mater. Phys.* **2001**, *64*, 075414.
(36) Yu, W.; Santiago-Aviles, J. J.; Furlan, R.; Ramos, I. Pyrolysis Temperature and Time Dependence of Electrical Conductivity Evolution for Electrostatically Generated Carbon Nanofibers. *IEEE T. Nanotechnol.* **2003**, *2*, 39−43.
(37) Wang, Y.; Serrano, S.; Santiago-Avilés, J. J. Raman Characterization of Carbon Nanofibers Prepared Using Electrospinning. *Synth. Met.* **2003**, *138*, 423−427.
(38) Jung, S.; Lee, J.; Hyeon, T.; Lee, M.; Kim, D.-H. Fabric-Based Integrated Energy Devices for Wearable Activity Monitors. *Adv. Mater.* **2014**, *26*, 6329−6334.
(39) Pu, J.; Wang, X.; Xu, R.; Komvopoulos, K. Highly Stretchable Microsupercapacitor Arrays with Honeycomb Structures for Integrated Wearable Electronic Systems. *ACS Nano* **2016**, *10*, 9306−9315.
(40) Diaz, A. F.; Felix-Navarro, R. M. A Semi-Quantitative Tribo-electric Series for Polymeric Materials: the Influence of Chemical Structure and Properties. *J. Electrost.* **2004**, *62*, 277−290.
(41) Jestrović, I.; Coyle, J. L.; Sejdić, E. Decoding Human Swallowing via Electroencephalography: A State-of-the-Art Review. *J. Neural Eng.* **2015**, *12*, 051001.

DOI: 10.1021/acsami.8b02564
ACS Appl. Mater. Interfaces 2018, 10, 15855−15863